

Convex Mapping Formulations Enabling Optimal Power Split and Design of the Electric Drivetrain in All-Electric Vehicles

Arne De Keyser¹, Matthias Vandeputte, and Guillaume Crevecoeur

Abstract—All-electric drivetrains have been identified as a promising alternative to contemporary hybrid vehicle technology. Extending their operational range is key and can be achieved by means of design procedures based on high-fidelity models capturing the dynamical behavior of the electric drivetrain. This paper proposes a dedicated power split embodying a dual electric drive and a model-based strategy to design the drivetrain. Advancements are required in model-based design that can cope with the complexity of the computationally expensive and high-dimensional parametric design problems. We propose a nested optimization approach wherein parameter exploration is attained using an evolutionary algorithm and the optimal power flows are determined by abstracting the high-fidelity behavioral models into appropriate convex loss mappings. This allows for an accelerated design procedure based on convex optimization without compromising accuracy. We size an electric drivetrain for maximal range extension, consisting of a battery stack, buck-boost converter, inverter and mechanically coupled induction motors subjected to variable load conditions. A tractable convex formulation is obtained and optimization time is reduced by 99.3% compared to the traditional approach without convexification. Optimal control of the incorporated power split increases the operational range by 0.7% compared to the isolated operation of a single motor. The proposed methodology thus paves the way for extensive designs of drivetrains and complex mechatronic systems in a general context.

Index Terms—Convex functions, design optimization, electric vehicles, mechatronics, metamodeling.

I. INTRODUCTION

COMPLEX dynamic systems necessitate dedicated resources and specific methodologies, especially in the highly variant and flexible environments encountered in mechatronic design problems. A specific class within the general

domain of mechatronic engineering consists of electric energy conversion, revolving around the power flows between distinct components. All-electric drivetrains provide a promising alternative to contemporary combustion-based technology with the aim of reducing harmful emissions. Model-based design of such complex mechatronic systems involves a multitude of high-fidelity models acting on various domains (electric, mechanical, etc.) and time scales. Contemporary numerical design procedures [1], [2] often entail an intrinsic deficiency in terms of time-efficient and objective-focused model abstraction. To enable tractable model-based design from computational time perspective as well as to reduce the observed complexity in the design phase, a streamlined approach is needed wherein high-fidelity models and corresponding control structures are abstracted. Translation of the problem into a suitable and highly time-efficient solver can be made possible by reducing the complexity associated to the multitude of models, elevated dimensionality of the parameter space and various distributed controllers.

A general revision of the standard and demanding numerical optimization procedures, mostly employing the computationally expensive dynamic programming [3] and related methodologies [4], was proposed on the basis of the principles of convex optimization in [5]. Convex solvers are known to converge in polynomial time and are able to cope with a vast amount of equality and inequality constraints. This benefit can be further exploited by formulating a convex sizing procedure [6]. Furthermore, heuristic rules can be determined founded on a more intuitive approach, being of purely deterministic [7] or fuzzy nature [8]. A big detriment to this framework is the lack of analytical foundation and ability to prove the asserted optimality. Parameter exploration based on evolutionary algorithms [9], [10] allows for both exploration of the design space and exploitation of favorable regions based on the unambiguous evaluation of the design cost.

To extend the operational range of currently existing electric drivetrains for vehicular technology, one can resort to a model-based design approach that needs to cope with the complexity and curse of dimensionality [11]. We explore a power split embodied as a dual electric drive and perform a model-based design with respect to this electric drivetrain. The proposed technology enables exploitation of distinct operating regions, analogous to the concept of hybrid drivetrains, in terms of energy efficiency. Dynamical power losses need to be mapped as

Manuscript received November 7, 2016; revised June 28, 2017; accepted August 16, 2017. Date of publication August 25, 2017; date of current version November 10, 2017. This work was partially supported by the strategic basic research project EMODO of Flanders Make, the Strategic Research Centre for the Manufacturing Industry; the BOF 01N02716 and BOF 01D37816 project; and the FWO research project G.0D93.16N. The review of this paper was coordinated by Mr. D. Diallo. (Arne De Keyser and Matthias Vandeputte contributed equally to this work.) (Corresponding author: Arne De Keyser.)

The authors are with the Department of Electrical Energy, Metals, Mechanical Constructions and Systems, Ghent University, 9000 Ghent, Belgium, and also with Flanders Make, the Strategic Research Centre for the Manufacturing Industry, Belgium. (e-mail: arndkeys.DeKeyser@UGent.be; Matthias.Vandeputte@UGent.be; Guillaume.Crevecoeur@UGent.be).

Color versions of one or more of the figures in this paper are available online at <http://ieeexplore.ieee.org>.

Digital Object Identifier 10.1109/TVT.2017.2745101

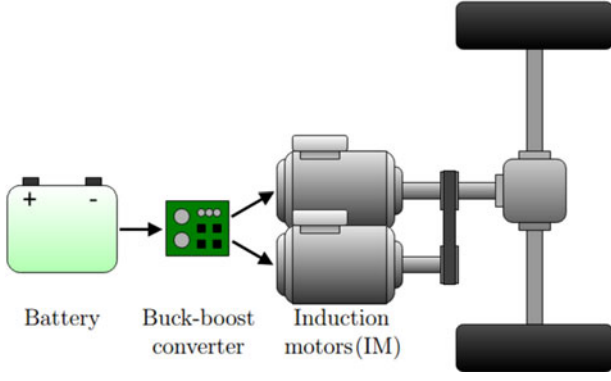


Fig. 1. Proposed drivetrain design with two distinct asynchronous motors in power split. Separate voltage source inverters supply the motors.

a function of power flows, which can constitute the basis for time-efficient power flow distribution and the resulting power splitting between drives. Based on the criteria for operation, optimal operating scenarios can be generated for a specific set of design parameter values. A nested optimization strategy is therefore proposed, consisting of an inner loop determining the optimal power flow variables and an outer loop assessing the sizing parameters with respect to a predominating objective. The dynamics of the system under design are incorporated in the convex mappings that are function of the underlying state variables, e.g. input and output power flows, stored kinetic or potential energy, etc. No trade-off between time-saving measures and level of accuracy needs to be consulted as the convex mappings can be directly deduced from high-fidelity physics-based models. The effectiveness of the proposed design strategy is demonstrated based on a case study concerning the domain of vehicle technology, namely an all-electric vehicle incorporating dual propulsion drives.

II. OBJECTIVE-ORIENTED CONVEX MAPPINGS

A first step in the pursuit of an effective design consists of translating the high-fidelity models, in which the dynamic behavior of the components composing the complete mechanism is contained, into a formulation suited for minimization within the framework of convex optimization. Abstraction of the detailed models is therefore inevitable but despite the corresponding loss of physical representation, the abstracted models allow for a time-efficient optimization procedure.

A basic lay-out for electric propulsion has been carried out, consisting of a battery stack [12], a DC-DC converter [13], a voltage source inverter (VSI) [14], two distinct cooperating asynchronous machines [15] and a fixed final reduction as depicted in Fig. 1. A detailed discussion regarding the physical modeling of the interconnected system is gathered in Appendix A.

The accommodated energy is provided by the battery stack, while a buck-boost converter with its corresponding PID-control provides a controllable voltage level. Consequently, a voltage source inverter converts the DC voltage level to an appropriate 3-phase voltage system. The provided torque of the distinct machines is controlled by direct torque control [16]. The ob-

jective of the optimization consists of enhancing the vehicle's operating range by sizing the battery stack and electing a favorable combination of drives. Note that the drivetrain in Fig. 1 can be implemented for various industrial applications where a varying load needs to be driven. The driveline component models are elaborated in Appendix A. The physical characteristics of the battery, DC-DC converter and the mechanical driveline are assumed to be fixed quantities. All decisive numerical parameters are included in Table II of Appendix C. Furthermore, setpoints for the voltage reference (V_{set}) and flux level (Ψ_{set}) are also provided. Both voltage and flux reference can furthermore be incorporated in a supervisory control loop [17]. This is however out of the scope of this article. Finally, the component values for the dynamical models of the induction motors under consideration are listed in [18].

A. Model Abstraction Into Convex Mappings

A special class within the broad concept of mathematical functions consists of so-called convex functions with its specific particularities. Since a local optimum of a convex minimization problem is also the global optimal solution, one can combine the minimization of convex costs for all component modules in the interconnected system. Furthermore, the sum of distinct functions, each of them being convex in the considered variables, remains convex, which allows for summation of different objectives. More information concerning the background of convex functions and their practical use within optimization problems can be found in [19]. For the actual implementation in a numerical environment, the MATLAB package CVX was used [20], [21].

The main goal of the sizing procedure is to minimize the total system's cost $C(\cdot)$ which is intrinsically connected to the dynamic behavior of a certain design with respect to the predominating criteria, assessed by the convex cost function $L(\cdot)$. Both minimization problems are restricted by constraints indicating the feasible region, for which linear constraints are denoted by the matrices $\mathbf{A} \in \mathbb{R}^{n_a \times n_p}$, $\mathbf{A}_{\text{eq}} \in \mathbb{R}^{n_b \times n_x}$, $\mathbf{b} \in \mathbb{R}^{n_a}$ and $\mathbf{B}_{\text{eq}} \in \mathbb{R}^{n_b \times n_t}$ whose dimensions depend on the amount of linear constraints imposed in the outer (n_a) or inner ($n_b \cdot n_t$) optimization loop. Furthermore, m convex boundaries are incorporated in the set of functions $g_j(\cdot)$ ($j = 1, \dots, m$). A generalized formulation of the problem statement for a time horizon $\mathbf{t} \in \mathbb{R}^{n_t}$ is presented in (1).

$$\begin{aligned}
 \mathbf{p}^* &= \arg \min_{\mathbf{p}} C(\mathbf{p}, L^*(\mathbf{p})) \\
 \text{s.t. } &\mathbf{A}\mathbf{p} \leq \mathbf{b} \\
 \text{s.t. } &L^*(\mathbf{p}) = \min_{\mathbf{X}} L(\mathbf{p}, \mathbf{X}) \\
 \text{s.t. } &\begin{cases} \mathbf{A}_{\text{eq}}\mathbf{X} = \mathbf{B}_{\text{eq}} \\ g_j(\mathbf{X}) \leq 0 \text{ for } j = 1, \dots, m \end{cases} \\
 &\text{with } L(\mathbf{p}, \cdot) \text{ and } \{g_j(\cdot)\} \text{ convex.} \quad (1)
 \end{aligned}$$

The characterizing state variables for each time step are herein represented by $\mathbf{X} \in \mathbb{R}^{n_x \times n_t}$, while the vector $\mathbf{p} \in \mathbb{R}^{n_p}$ contains the distinct parameters for the tuning procedure. In the

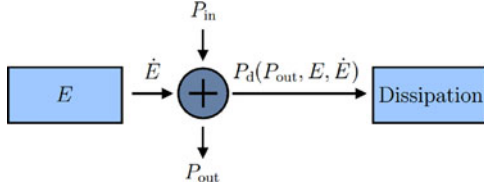


Fig. 2. Overview of the power flows in a node of the system.

introduced case study, the internal states of the system depict the input and output power flows and the stored energy for each distinct component. Conservation of energy transferred from one component to the next results in linear equality constraints included in the expression $\mathbf{A}_{eq}\mathbf{X} = \mathbf{B}_{eq}$.

In the treated application, the original state space matrices in torque, speed, voltages and currents are not state-invariant. Therefore a translation to the convex problem statement in the form of a linear state space model is not directly applicable. The observed nonlinearities are induced by the speed-dependency of the state evolution for the asynchronous machines. A power-oriented abstraction is made and the system power flows and energy buffer states are chosen as state vector elements. Hence, the state space equations resulting from the conservation of energy are time invariant. The proposed formulation could nevertheless be variant in time, given that the characteristic system matrices \mathbf{A}_{eq} and \mathbf{B}_{eq} are not a function of the states. Linearity of the equality constraints needs to be maintained.

The time instant is not explicitly specified for the convex boundaries in (1) such that the internal relations or the objective performance can be a function of previous states. This enables us to translate a power flow model containing time derivatives to the convex problem statement by approximating the derivative operators by forward or central differencing.

B. Convexification of the Power Flows

A correct objective-oriented mindset plays a major role in obtaining an effective implementation of the proposed algorithm as the system dynamics need to be casted into an objective function L . The operating range of the all-electric vehicle constitutes the focal point of the work presented in this paper, which corresponds to a minimization of the energy leaving the battery stack. Therefore, power and energy flows can be considered as the decisive factor within the complete configuration. A generalized formulation of the power balance can be expressed as the equality of all incoming and leaving flows (2).

$$P_{in} + \dot{E} = P_{out} + P_d. \quad (2)$$

This expression can be translated into a schematic nodal representation of the power flows in a node of the system based on [5], as demonstrated in Fig. 2.

The output power (P_{out}) results directly from the external demands on the system, while the change of stored energy (\dot{E}), e.g. kinetic energy, can be deduced from the system configuration at each time instant. All power flows, and consequently all changes in energy, are thus uniquely defined if mappings of the dissipation (P_d) in each component or subsystem are con-

structed. As power losses tend to monotonously increase when deviating from optimal operation, a model abstraction of the dissipated power into a convex mapping-based formulation is intuitively feasible. In (2) the dissipative flows can be formulated as a convex function f of the other power flows and the stored energy in the junction.

$$P_{in} = P_{out} - \dot{E} + f(P_{out}, E, \dot{E}). \quad (3)$$

To prove the existence of a convex reformulation, one can consider the power flows associated with the electric motor. As the change in internal energy is assumed to be negligible with respect to the provided mechanical power, (3) is rewritten as:

$$P_{in} = P_{out} + P_d. \quad (4)$$

In order to satisfy the conditions proposed in the convex problem formulation (1), this equality needs to be relaxed into an inequality constraint.

$$P_{in} \geq P_{out} + P_d. \quad (5)$$

P_d is uniquely defined for a certain output power P_{out} and because of (4) also for a certain input power P_{in} . Assuming \tilde{P}_{in} to be the optimal solution for P_{in} coinciding with this convex inequality constraint and another solution P_{in} satisfying the inequality constraint (5), one can write:

$$\begin{aligned} P_{in} &= \gamma + P_d(P_{in}) + P_{out} \\ &= \gamma + P_d(\tilde{P}_{in} + \gamma) + P_{out} \\ &\triangleq \gamma + P_d(\tilde{P}_{in}) + \Delta P_d + P_{out}. \end{aligned} \quad (6)$$

With γ being a non-negative real-valued slack variable and ΔP_d the change in the power dissipation when deviating the input power P_{in} from its optimal solution \tilde{P}_{in} . Taking the equality relation in (4) into account, the following relation can be obtained:

$$P_{in} = \tilde{P}_{in} + \gamma + \Delta P_d. \quad (7)$$

For which \tilde{P}_{in} is optimal if and only if the following condition holds:

$$\gamma + \Delta P_d \geq 0. \quad (8)$$

Consequently the reformulation in a relaxed convex problem results in a solution coinciding with the boundary of the inequality constraint and thus satisfying the original equality constraint. As ΔP_d is previously defined as

$$\Delta P_d = P_d(P_{in} + \gamma) - P_d(P_{in}). \quad (9)$$

It immediately follows that

$$\begin{aligned} |\Delta P_d| &= \gamma \left| \frac{P_d(P_{in} + \gamma) - P_d(P_{in})}{\gamma} \right| \\ &\leq \gamma \left| \left[\frac{\partial P_d}{\partial P_{in}} \right]_{\max} \right|. \end{aligned} \quad (10)$$

Plugging this result in (8) and reminding that γ is non-negative, consequently leads to

$$1 \geq \left| \left[\frac{\partial P_d}{\partial P_{in}} \right]_{\max} \right|. \quad (11)$$

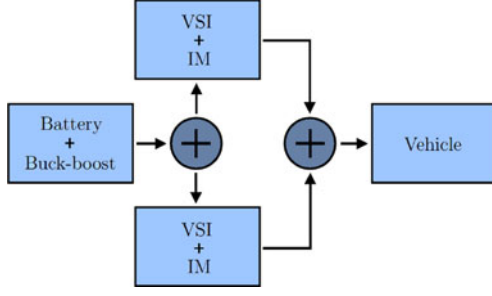


Fig. 3. Reduced subsystem-focused representation of the proposed drivetrain.

Therefore, a sufficient condition for the applicability of the aforementioned relaxation is formulated.

$$-1 \leq \frac{\partial P_d}{\partial P_{in}} \leq 1. \quad (12)$$

This condition is intuitively weak, as this translates in an increase of the dissipated power that outweighs the increase in transferred mechanical power. In a practical context, this operation is to be avoided. One can thus assert that the practical operating range is restricted to the area of monotonous increase, which satisfies the imposed requirements for a convex optimization procedure. A completely similar methodology can be developed for the energy supply, in which P_{in} should be replaced by \dot{E} , as only an internal charge is present.

The followed approach can thus be applied in a generic manner to electric drivetrains and convex mapping formulations. In order to ensure convexity and to reduce the number of necessary convex loss models, components are merged into separate subsystems, which can be seen in Fig. 3, providing a schematic overview of the studied drivetrain.

With respect to the energy supply, including both battery and buck-boost converter, the loss model is initially parametrized in the magnitude of the stack n . The corresponding surface $P_{b,d}$ appears to be convex as a function of the variables E_b and $P_{b,out}$, as proposed in [5]. Convex loss models, coupled with the stack size n through the coefficients of the regression and characterized by (13) can thus be constructed. A parabolic dependency on the supplied power is proposed, while the influence of the actual energy level is assumed to behave in a linear trend.

$$P_{b,d} = a_n P_{b,out}^2 + b_n P_{b,out} + c_n E_b + d_n. \quad (13)$$

Herein the notation E_b is wielded to denote the accommodated energy in the battery cells, while $P_{b,out}$ represents the power leaving the supply unit at the output of the DC-DC converter. The resulting surface and its convex approximation for a connection of 330 NiMH-cells [12] are provided in Fig. 4.

A least-squares calculation provides the coefficient values for the convex approximation, with reference data for regime power and losses being provided by high-fidelity simulations of the isolated subsystem with a simulation time span of 0.1 s and a step size equaling 50 μ s. The underlying analytical models for the distinct components are covered in Appendix A. A total of 301 high-fidelity simulations of an isolated battery-converter module with varied current draw suffices to construct a reliable convex loss model.

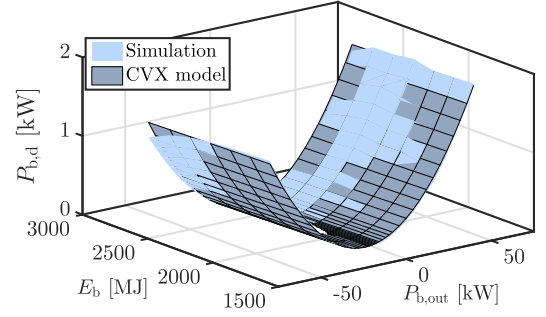


Fig. 4. Convex model of the dissipation $P_{b,d}$ for an energy supply containing 330 NiMH-cells.

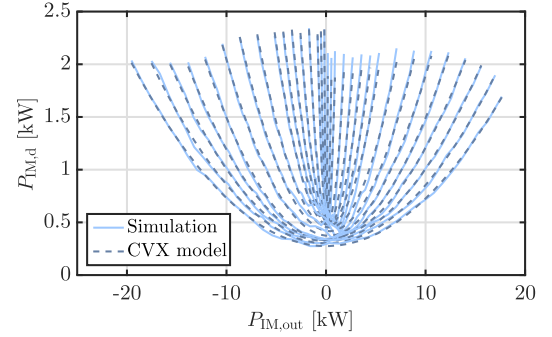


Fig. 5. Convex model of the dissipation $P_{IM,d}$ for an asynchronous motor of 19 kW with its corresponding supply. The quadratic coefficient decreases monotonously for higher ω .

The asynchronous motor and its three-phase supply can be mapped by introducing varying torque reference and rotational speed signals, hereby altering the output power of the propulsion mechanism. The flux setpoint in the control algorithm is fixed at a level of 1.0 Wb, while a constant input voltage of 400 V is furthermore assumed as this quantity is internally controlled. Within this approach, the different convex loss mappings are parametrized for various rotational speeds ω . For each imposed speed a quadratic relation $f_\omega(P_{IM,out})$ for the dissipated power $P_{IM,d}$ is determined with $P_{IM,out}$ being the output power of the subsystem. The other power and energy variables, i.e. E and \dot{E} , are unambiguously defined if an external speed profile (subscript ω in (14)) and the corresponding kinetic energy variations are imposed.

$$P_{IM,d} = a_\omega P_{IM,out}^2 + b_\omega P_{IM,out} + c_\omega. \quad (14)$$

In order to minimize the expected quadratic error between the simulated data points and the parabolic approximation, a standard least-squares algorithm provides the optimal estimates for the different model coefficients in (14). An example to demonstrate the validity of the incorporated mapping is given in Fig. 5, displaying the curves for a machine with a rated power of 19 kW [18]. The reference steady state data are obtained based on 1312 short-term simulations of the computationally expensive models provided in Appendix A over a period of 0.1 s with a discrete simulation step of 50 μ s.

If convex estimates need to be provided at intermediate speeds, linear interpolation between the surrounding mappings

is executed. This methodology can be justified by considering the monotonous behavior of the quadratic approximations as a function of the rotational speed, as displayed in Fig. 5.

C. Equivalent Convex Problem Statement

Given these convex formulations of the dissipation in each subsystem, the complete problem statement can then be transformed into an expression matching (1) and subsequently implemented in the environment of a convex solver. Referring to the problem statement presented in (1), the convex formulation is implemented for the dual drive based on the occurring energy flows in the drivetrain and the corresponding dissipation mappings. The complete state \mathbf{X} contains all power transfers at each time instant. All power flows in the system, which is reduced to a connection of several mapped subsystems, are determined over the complete optimization horizon. The input to the system consists of the requested output power P_{req} , imposed by the external load. Based on the calculated power flows, the optimal distribution between both electric machines is immediately assessed. If one takes the external velocity profile into account, the optimal torque references over the course of the trajectory are uniquely defined.

The implemented minimization problem for a sampling time Δt is written as:

$$L^* = \min_{\mathbf{X}} \sum_{k=1}^{n_t} \dot{E}_b(k) \cdot \Delta t$$

$$\text{s.t.} \begin{cases} P_{b,\text{out}}(k) - P_{\text{IM1},\text{in}}(k) - P_{\text{IM2},\text{in}}(k) = 0 \\ P_{\text{drive},\text{in}}(k, \mathbf{p}) - P_{\text{IM1},\text{out}}(k) - P_{\text{IM2},\text{out}}(k) = 0 \\ P_{\text{req}}(k, \mathbf{p}) - P_{\text{drive},\text{out}}(k, \mathbf{p}) = 0 \\ P_{b,d}(k) + P_{b,\text{out}}(k) - \frac{E_b(k) - E_b(k-1)}{\Delta t} \leq 0 \\ P_{\text{IM1},d}(k) + P_{\text{IM1},\text{out}}(k) - P_{\text{IM1},\text{in}}(k) \leq 0 \\ P_{\text{IM2},d}(k) + P_{\text{IM2},\text{out}}(k) - P_{\text{IM2},\text{in}}(k) \leq 0 \\ P_{\text{drive},d}(k) - (1 - \eta^{\text{sgn}(P_{\text{drive},\text{in}}(k))}) P_{\text{drive},\text{in}}(k) \leq 0. \end{cases} \quad (15)$$

The governing equality and inequality constraints can be casted into a formulation matching (1), introducing the appropriate matrices \mathbf{A}_{eq} , \mathbf{B}_{eq} and functions g_j respectively. In this set of equations, an additional quantity P_{drive} is introduced, which denotes the power flow to the mechanical part of the driveline with a fixed efficiency η equaling 90%. The incorporated inequality constraints signify the relaxed constraints following from the conservation of energy passing through and dissipated in each component, while the equalities indicate the physical connection between components, as denoted in Fig. 3. The chosen objective function, being the time integral of the energy leaving the buffer, is positive and linear in the states of the system and is thus a strictly increasing convex function of the battery buffer state E_b over time.

III. EMBEDDING CONVEX MAPPINGS FOR SIZING

In order to obtain an ideal configuration with a minimal value for the design cost $C(\cdot)$, different feasible designs and their respective set of sizing parameters \mathbf{p} need to be evaluated and

compared with respect to each other in terms of the objective. The characteristic parameters determine the dimensions, behavior and costs of the components. Altering these characteristics allows to explore different feasible regions. In contrast to [5], convex optimization for the sizing procedure is discarded, as this would inhibit the possibility to include different types of electric motors. Furthermore, only a limited library of reference components is used in the course of this work and a reliable assessment of a possible sizing trend is therefore not feasible.

An effective search algorithm combines exploration, as to include every area in the design space, with exploitation, i.e. elaborating further on promising designs by slightly adjusting the characteristic parameters. In order to satisfy the proposed needs, the genetic search is elected [22]. This evolutionary algorithm is able to cope with discrete variables, which in this case represent the limited set of induction motors in the library. In order to guarantee the general applicability of the approach, the standard mixed integer genetic search algorithm of Matlab, MILXPM, is implemented [23]. An observable trend in the mapped motor characteristics would furthermore favor a faster convergence. The number of batteries in the stack is approximated by a continuous variable and eventually rounded to the closest integer value. Nevertheless, other global search heuristics can be engaged in the design procedure.

In the evaluation step of the search algorithm, which is iteratively repeated during the evolutionary search, the fitness of each population member is assessed. As this step is to be repeated during each iteration and for every offspring, a time-efficient approach is desired. For each configuration elected by the search algorithm, and the corresponding set of parameters \mathbf{p} , the fitness is obtained by convex optimization of the power flow system in terms of energy efficiency. The total cost $C(\cdot)$ for each design can be constructed as the sum of different objectives, where one can combine the energy dissipation during optimal operation (L^*) with additional (virtual) costs, e.g. denoting accelerated wear or elevated investments in machinery. For the proposed case study (15), the fitness is solely assessed based on energy considerations.

IV. RESULTS AND DISCUSSION

The introduced application provides valuable insights with respect to the numerical performance of the proposed algorithmic structure regarding accuracy and time-efficiency. The ideal configuration of the interconnected system is prone to changes, taking into account that only a limited library of reference components is used and thereby mapped in their respective convex loss approximations. Furthermore, only an internal series connection of the battery stack is considered. Parallel energy buffers can be readily incorporated, in which each battery pack has to deliver only a predefined fraction of the output power, based on the ratios of the branch resistances.

A. Algorithmic Results

To assess the performance of the proposed procedure, both the necessary calculation time and the corresponding number of iterations are consulted for problems with a stepwise increase in

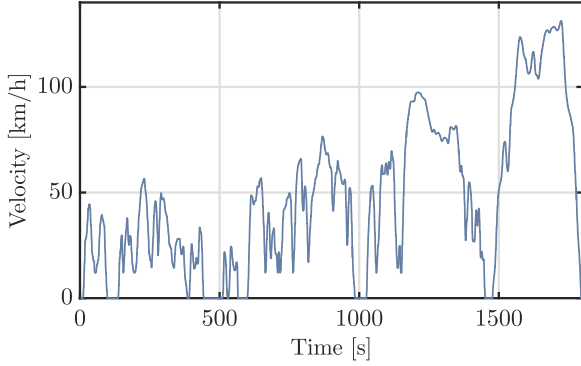


Fig. 6. Standardized velocity profile of the WLTP (Class 3) reference cycle.

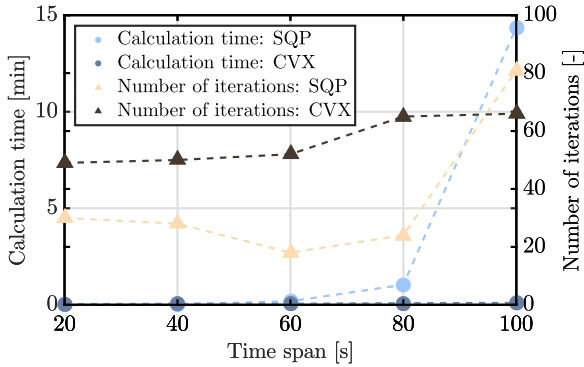


Fig. 7. Calculation time and number of iterations (SQP and CVX) for increasing problem dimensions.

time span and thus total dimension. In a first phase, the power split between the engines is optimized over the standardized WLTP road cycle provided in Fig. 6, ranging from a duration of 1 s up until 100 s. The actual power demand at each time instant is determined using an analytical model of the vehicle dynamics, which is included in Appendix B.

The performance of the approach based on objective-oriented convex mappings is compared to a classical Sequential Quadratic Programming (SQP) solver in MATLAB (R2015b; Mathworks, Natick, MA, USA). As is demonstrated in Fig. 7, the total computational time for the standard minimization procedure rises in an exponential way, the so-called curse of dimensionality associated to $\min_{\mathbf{X}} L(\mathbf{p}, \mathbf{X})$. The dimensionality of \mathbf{X} ranges from 381 for a limited time span of 20 s up to 1901 for an optimization horizon of 100 s. Convex mappings on the other hand allow to limit the necessary time drastically, more specifically by 99.3%. The construction of the necessary convex formulations needs some supplementary preprocessing, but needs to be carried out only once for a single subsystem. Furthermore, these mappings can be computed in advance. The increased calculation times are due to the rising number of iterations to find $L^*(\mathbf{p})$ for longer time horizons, both for SQP and CVX. For even longer time horizons, the SQP-algorithm fails to find a feasible solution in a reasonable time, since the dimensionality becomes larger than what's practically achievable. This discards the possibility to include more than 100 time

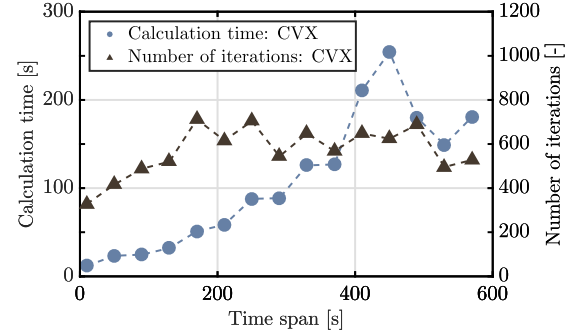


Fig. 8. Calculation time and number of iterations (CVX) for lengthy time spans.

steps within the actual sizing procedure and therefore impedes a drivetrain design based on a representative reference cycle.

As demonstrated in Fig. 8, the convex abstraction allows to determine optimal operation for extended time spans, i.e., larger than 500 time steps, thereby enabling a sizing procedure of the proposed system. Assessment of the optimal sizing parameters \mathbf{p}^* based on standard optimization strategies would be out of the question, as the mentioned minimization associated to $L^*(\mathbf{p})$ is repeated for each evaluation step in the iterative approach.

The number of iterations necessary to converge to the optimal solution does not increase monotonously. The convex optimization procedure thus efficiently selects the next best guess for the optimal solution. For longer time spans, one would intuitively expect a higher calculation time, which corresponds to the general trend observed in Fig. 8. The stable amount of iterations per number of considered time steps indicates that the increased total calculation time is mostly due to the increase in computational time per iteration. The observed variability in calculation time is associated with the specific translation into its respective convex problem formulation and the practical implementation of the internal solver.

B. Optimal Drivetrain Sizing

In the proposed case study, battery stack size is varied to allow for higher initial charge but comes with an inherent increase in mass, assumed to be 170 g per additional cell. Therefore including an additional energy reservoir leads to extended vehicle range but possibly suboptimal operation due to the increased weight and corresponding rise of inertial forces to be overcome. The collection of propelling motors is chosen to be a limited selection of induction motors with two pole pairs, spanning a whole range of distinct rated powers [18]. Furthermore, the asynchronous machines are assumed to have a constant specific power ρ_{IM} equal to 1.5 kg/kW. This measure discourages equipping over-sized motors in the design if this results in no significant improvement of the performance. To explore the design space, a population size of 8 is chosen and the maximum number of iterations is fixed at 15, while all other settings are kept at their default conditions. The small values for the characteristic parameters stem from the limited amount of possible configurations, which will cause the genetic search to converge rapidly.

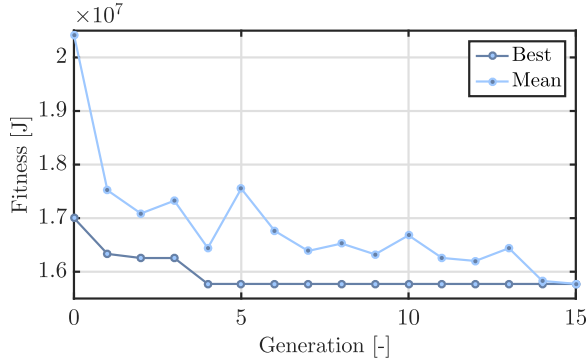


Fig. 9. Convergence plot of the genetic sizing procedure for an initial population of eight members.

TABLE I
OPTIMAL DRIVETRAIN CONFIGURATION

Parameter	Value
E_{max}	665.6 kW·h
$P_{n,1}$	75 kW
$P_{n,2}$	19 kW

During the sizing procedure, the genetic algorithm steadily converges towards an optimal configuration, minimizing the occurring drop in available energy over a standardized trajectory as depicted in Fig. 9. On this graph, the presented fitness function corresponds to the total consumed energy during the road cycle. This quantity reaches a minimum after five generations, while the mean cost remains at a higher level, demonstrating the further attempts to explore the whole parameter space. Based on the provided convergence graph, one could conclude that a, at least close to, optimal configuration has been achieved. The complete sizing procedure is terminated in 12 h 43 min on an Intel i7-6600U processor for a reference cycle spanning 30 min. Each evaluation of the convex problem statement (15) necessitates the determination of 34 196 variables, subject to a total of 16 197 constraints and is finished in approximately 478 s. The vector of sizing parameters \mathbf{p} has a dimension of three in the representative case, as three characteristics of the drivetrain are variable and can thus be altered towards an optimal configuration.

An optimal energy buffer results in a stack containing 302 cells of the proposed NiMH-battery, while cooperating drives of 37 and 132 kW prove to operate in the most favorable fashion regarding energy management of the accommodated battery charge. The obtained optimal design is outlined in Table I. The corresponding maximal energy buffer, in the fully charged state, is denoted by E_{max} . Furthermore, rated powers for both asynchronous machines are represented by $P_{n,k}$ ($k = 1, 2$).

Optimal control of the power flows in both engines improves the energy management of the battery with 0.7%, compared to isolated operation of the main propulsion motor. The actual power split between both asynchronous motors is demonstrated in Fig. 10. As can be observed, the smaller engine provides the

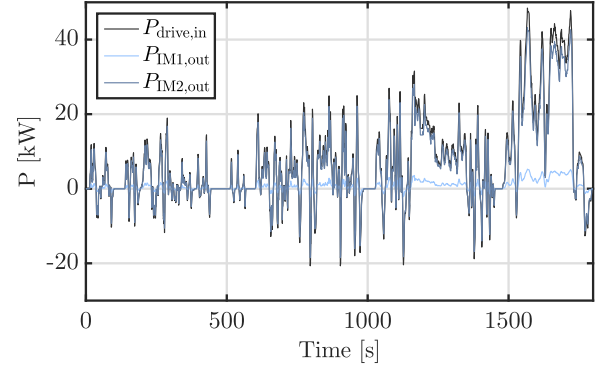


Fig. 10. Distribution of the demanded output power $P_{IM,out}$ of both induction motors over the complete trajectory.

majority of the power at low power demands, while the reverse situation is noticed during intervals of elevated power consumption. The only minor improvement is caused by the absence of a discrete on-off management heuristic [24] for both motors, which could eliminate losses at zero load. As these losses add up to a considerable fraction of the total power dissipation, including a supervisory control loop can thus significantly improve the collaboration between both engines. This constitutes the topic of future research.

Similar graphs can be obtained for all power flows occurring in the drivetrain. These flows rely solely on the implemented constraints as the power split and corresponding torque distribution is the subject of the optimization procedure.

V. CONCLUSION

A model-based design approach for attaining optimal power split and design of the electric drivetrain in all-electric vehicles is presented. The main objective is to increase the operational range of an optimally sized dual drive topology consisting of two asynchronous motors that can serve in different operating conditions. This configuration is proposed to anticipate for varying load conditions, allowing for a more efficient usage of the accommodated energy. Due to the complexity and the high dimensionality of the parameter space, advancements of the model-based design procedure are required. A nested design optimization approach, combining time-efficient computations with high-fidelity physics, is proposed based on specific convex abstraction towards the design objective. Convex models are preferred, as these allow to implement the principles of convex optimization and benefit from its computational time-efficiency. A combination with a genetic search is introduced as to include exploration of feasible designs. Results with respect to both optimal design and the design procedure itself are considered, comparing the observed performance to that of classic algorithms employed within the domain of vehicular technology. Based on the proposed procedure, the design problem is rendered tractable and optimization time is reduced by 99.3% with respect to a standard SQP-minimization procedure. Optimal power distribution allows to improve the energy management of a single battery charge by 0.7%. The limitation on the observed improvement stems from the absence of a

supervisory on/off management strategy. Nevertheless, the proposed framework, with a special focus on convex abstraction of system-specific behavior, outperforms the classical approach for lengthy time horizons. It is therefore primarily appealing for the complex engineering problems encountered in mechatronic environments.

APPENDIX A HIGH-FIDELITY COMPONENT MODELING

A. Battery Stack

The output voltage of standard battery types reduces as the state of charge (SOC) depletes. The voltage-SOC relation shows to be highly non-linear for charging over around 80% of the maximum capacity or discharging under around 20% of the highest possible charge to be held by the battery. In [12] these non-linear sections are expressed as a rational and exponential curve added to the approximately linear voltage-discharge relation. For a known evolution of the current through the battery (i_b), this leads to:

$$e(t) = e_0 - K_1 \cdot \frac{Q}{Q - \int_0^t i_b d\tau} + K_2 \cdot e^{-K_3 \cdot \int_0^t i_b d\tau}. \quad (16)$$

In this equation $e(t)$ denotes the internal voltage of the battery cell with maximal charge Q . The parameters K_1 , K_2 and K_3 in the proposed expression can be deduced from data provided by the manufacturers. Incorporating the internal resistance R_i , which is often non-negligible and introduces dissipation, leads to an output voltage reduced by the corresponding voltage drop. The values used for the high-fidelity simulation for several battery types are inspired by [12]. The respective numerical values are summarized in Table II.

B. DC-DC Converter

A state-space representation for a converter fed by a constant but variable voltage source v_b at the input and connected to a load with a known current i_{BB} drawn at the output is derived. The characteristic inductance L_{BB} and capacitance C_{BB} demonstrate parasitic dissipative effects, introduced by the resistances R_L and R_C . The state derivatives for inductor current i_L and capacitor voltage v_C are approximated by weighing the relative duration of the switching states of the converter using the duty ratio δ . For boost-operation, this results in:

$$\dot{\mathbf{x}}_{BB} = \mathbf{A}_{BB}\mathbf{x}_{BB} + \mathbf{B}_{BB}\mathbf{u}_{BB}. \quad (17)$$

With

$$\begin{aligned} \dot{\mathbf{x}}_{BB} &= \begin{bmatrix} \dot{i}_L \\ \dot{v}_C \end{bmatrix}; \mathbf{u}_{BB} = \begin{bmatrix} v_b \\ i_{BB} \end{bmatrix}; \\ \mathbf{A}_{BB} &= \begin{bmatrix} -\frac{R_L}{L_{BB}} + \delta \frac{R_C}{L_{BB}} & -\delta \frac{1}{L_{BB}} \\ \delta \frac{1}{C_{BB}} & 0 \end{bmatrix}; \\ \mathbf{B}_{BB} &= \begin{bmatrix} \frac{1}{L_{BB}} & \delta \frac{R_C}{L_{BB}} \\ 0 & -\frac{1}{C_{BB}} \end{bmatrix}. \end{aligned} \quad (18)$$

TABLE II
THE COMPONENT VALUES FOR THE HIGH-FIDELITY DRIVELINE SIMULATION

Parameter	Value
e_0	1.2848 V
R_i	0.0002 Ω
K_1	0.01875 V
K_2	0.144 V
K_3	$2.3077 (\text{Ah})^{-1}$
Q	6.5 Ah
m_b	170 g
ρ_{IM}	1.5 kg/kW
Ψ_{set}	1.0 Wb
$f_{switch,IM}$	20 kHz
L	130 μH
C	5 mF
R_L	0.0096 Ω
R_C	0.005 Ω
V_{set}	400 V
$f_{switch,BB}$	20 kHz
Parameter	Value
R_{CE}	0.005 Ω
$E_{sw,ref}$	0.01 J
I_{ref}	200 A
K_i	1
$V_{cc,ref}$	600 V
K_v	1.3
TC_{sw}	0.003
$T_{j,ref}$	150 $^{\circ}\text{C}$
f_{rol}	0.012
k_{rol}	0.0002 s^2/m^2
m_{car}	1000 kg
g	9.81 m/s^2
ρ_{air}	1.293 kg/m^3
SC_x	0.56
J_{wheels}	9.44 $\text{kg} \cdot \text{m}^2$
J_{drive}	1.2 $\text{kg} \cdot \text{m}^2$
i_e	1.01:1
r_{dyn}	0.3454 m

A similar model can be derived for operation in buck-mode. To control the transient behavior of the converter in a favorable manner and eliminate the steady state error on the output voltage, a basic PID-control loop is implemented. The corresponding gain factors are determined by application of the Ziegler-Nichols design methodology [25]. This way, both overshoot and settling time are reduced, while the steady state error is eliminated. The inherent power electronic components introduce additional losses in the system, being switching and conduction losses. These will be discussed in more detail in an upcoming section.

C. Induction Motor

The dynamic behavior of the induction motors is simulated by a fourth-order nonlinear state space model [15] in the different characteristic parameters, being stator resistance R_s , rotor resistance R_r , stator inductance L_s , rotor inductance L_r , mutual inductance L_m and number of pole pairs N_p . The mass of the induction motor is estimated by an empirical specific mass coefficient ρ_{IM} , such that $m_{IM} = \rho_{IM} P_{nom,IM}$, with $P_{nom,IM}$ the rated power.

In order to deliver the required torque within a reasonable region of accuracy, the direct torque control algorithm is implemented [16]. In problems dealing with stator control one usually

adopts a stationary reference frame. The state variables x are chosen to be the stator currents i_s and fluxes ψ_s in the complex plane. The real and imaginary components are denoted by a subscript x and y respectively. Based on predefined tables, the output torque and flux magnitude can be regulated to be confined in a limited hysteresis region around the respective reference values.

$$\dot{\mathbf{x}}_{\text{IM}} = \mathbf{A}_{\text{IM}}(\omega) \mathbf{x}_{\text{IM}} + \mathbf{B}_{\text{IM}} \mathbf{u}_{\text{IM}}. \quad (19)$$

With ω the rotational speed at the output shaft and

$$\begin{aligned} \dot{\mathbf{x}}_{\text{IM}} &= [i_{sx} \quad i_{sy} \quad \psi_{sx} \quad \psi_{sy}]^T \\ \mathbf{u}_{\text{IM}} &= [V_{sx} \quad V_{sy} \quad V_{rx} \quad V_{ry}]^T \\ \mathbf{A}_{\text{IM}}(\omega) &= \begin{bmatrix} \frac{L_r R_s + L_s R_r}{N} & -N_p \omega & -\frac{R_r}{N} & -\frac{L_r N_p}{N} \omega \\ N_p \omega & \frac{L_r R_s + L_s R_r}{N} & \frac{L_r N_p}{N} \omega & -\frac{R_r}{N} \\ -R_s & 0 & 0 & 0 \\ 0 & -R_s & 0 & 0 \end{bmatrix} \\ \mathbf{B}_{\text{IM}} &= \begin{bmatrix} -\frac{L_r}{N} & 0 & \frac{L_m}{N} & 0 \\ 0 & -\frac{L_r}{N} & 0 & \frac{L_m}{N} \\ 1 & 0 & 0 & 0 \\ 0 & 1 & 0 & 0 \end{bmatrix}. \end{aligned} \quad (20)$$

In this formulation the parameter N is defined by:

$$N = L_m^2 - L_r L_s. \quad (21)$$

No internal delays or parasitic effects are assumed in the inverter. However, power electronic losses are considered.

D. Switching Losses

Switching losses and conduction losses are observed in both the three phase voltage source inverter and in the DC-DC converter. Conduction losses are estimated by an equivalent collector-emitter resistance R_{CE} in the conducting path of the transistor. The switching losses per cycle, E_{sw} , are calculated by an approximate loss model of Semikron (22), a manufacturer of switching components.

$$\begin{aligned} E_{sw} &= E_{sw,ref} \left(\frac{I}{I_{ref}} \right)^{K_i} \left(\frac{V_{cc}}{V_{cc,ref}} \right)^{K_v} \\ &\times (1 + TC_{sw} (T_j - T_{j,ref})). \end{aligned} \quad (22)$$

Here $E_{sw,ref}$, I_{ref} , K_i , $V_{cc,ref}$, K_v , TC_{sw} and $T_{j,ref}$ are all reference and model parameter values provided in the component datasheet. V_{cc} denotes the supply voltage and T_j is the temperature at the junction. For both the DC-DC converter and the DTC-controlled induction motors, the switching frequency is fixed at 20 kHz.

APPENDIX B VEHICLE DYNAMICS

A. Dynamical Forces Acting on the Driveline

In order to propel the vehicle, different dynamical resistances have to be overcome, resulting in a counteracting torque. One can categorize two main components in the required torque,

being the rolling (23), drag (24) and inclination resistances imposed by the environment, and the acceleration torque for an acceleration a caused by the inertia of the vehicle (25). As a flat road is presumed, the presence of an inclination force is consistently disregarded. The friction coefficient for the rolling resistance is symbolized as f_{rol} , while k_{rol} denotes the speed dependency of the rolling resistance. The mass of the vehicle, m_{veh} is the sum of the car mass, m_{car} , induction motor masses m_{IM} and the mass of the battery stack m_b . The gravitational acceleration constant is incorporated by the notation g . Furthermore, the drag force F_{drag} is calculated using the volumetric mass density of air, ρ_{air} , the relative speed of the car compared to the surrounding air, V_{res} , and the drag coefficient SC_x .

$$F_{rol} = f_{rol} (1 + k_{rol} V^2) m_{veh} g \quad (23)$$

$$F_{drag} = \frac{1}{2} \rho_{air} V_{res}^2 SC_x \quad (24)$$

$$F_{acc} = k_m m_{veh} a. \quad (25)$$

The necessary torque has to be delivered by the pair of electric motors. Based on the desired acceleration, the internal control system can deduce the torque required to accelerate at a given rate, while the road dynamics impose the different counteracting forces. The inertia of the driveline is converted to an equivalent vehicle mass by adding a factor λ (26). The notation r_{dyn} corresponds to the dynamic wheel radius during driving.

$$k_m = 1 + \lambda = 1 + \frac{J}{m_{veh} r_{dyn}^2}. \quad (26)$$

With

$$J = J_{wheels} + i_e^2 J_{drive}. \quad (27)$$

The rotational kinetic energy stored in the drivetrain is obtained using the rotational inertia of the driveline components translated to an equivalent inertia at the motor axle (27) with i_e the differential gearing ratio.

B. Translation of Vehicle Dynamics to the Convex Problem Statement

Given the proposed formulation, the external loss functions are translated to a fixed output power flow $P_{drive,out}$. A generally acceptable approach to incorporate additional driveline losses is to assume a fixed efficiency η of 90%. Consequently, the dissipated power can be written as

$$P_{drive,d} = P_{drive,in} - P_{drive,out} = (1 - \eta) P_{drive,in} \quad (28)$$

when motoring ($P_{drive,in} \geq 0$) and

$$P_{drive,d} = P_{drive,in} - P_{drive,out} = \left(1 - \frac{1}{\eta}\right) P_{drive,in} \quad (29)$$

when regenerating energy ($P_{drive,in} < 0$).

APPENDIX C GENERIC PARAMETER VALUES

An overview of all constant numerical parameters for the different components composing the drivetrain is provided in Table II.

REFERENCES

- [1] E. Silva, T. Hofman, and M. Steinbuch, "Review of optimal design strategies for hybrid electric vehicles," *IFAC Proc. Volumes*, vol. 45, no. 30, pp. 57–64, 2012.
- [2] J. A. Reyer and P. Y. Papalambros, "Combined optimal design and control with application to an electric DC motor," *J. Mech. Design*, vol. 124, no. 2, pp. 183–191, 2002.
- [3] M. Koot *et al.*, "Energy management strategies for vehicular electric power systems," *IEEE Trans. Veh. Technol.*, vol. 54, no. 3, pp. 771–782, May 2005.
- [4] S. J. Moura, H. K. Fathy, D. S. Callaway, and J. L. Stein, "A stochastic optimal control approach for power management in plug-in hybrid electric vehicles," *IEEE Trans. Control Syst. Technol.*, vol. 19, no. 3, pp. 545–555, May 2011.
- [5] B. Egardt, N. Murgovski, M. Pourabdollah, and L. J. Mardh, "Electromobility studies based on convex Optimization: Design and control issues regarding vehicle electrification," *IEEE Control Syst. Mag.*, vol. 34, no. 2, pp. 32–49, Apr. 2014.
- [6] M. Pourabdollah, N. Murgovski, A. Grauers, and B. Egardt, "Optimal sizing of a parallel PHEV powertrain," *IEEE Trans. Veh. Technol.*, vol. 62, no. 6, pp. 2469–2480, Jul. 2013.
- [7] O. Sundström, L. Guzzella, and P. Soltic, "Torque-assist hybrid electric powertrain sizing: From optimal control towards a sizing law," *IEEE Trans. Control Syst. Technol.*, vol. 18, no. 4, pp. 837–849, Jul. 2010.
- [8] J. S. Won and R. Langari, "Intelligent energy management agent for a parallel hybrid vehicle Part II: Torque distribution, charge sustenance strategies, and performance results," *IEEE Trans. Veh. Technol.*, vol. 54, no. 3, pp. 935–953, May 2005.
- [9] V. Galdi, L. Ippolito, A. Piccolo, and A. Vaccaro, "A genetic-based methodology for hybrid electric vehicles sizing," *Soft Comput.*, vol. 5, no. 6, pp. 451–457, 2001.
- [10] S. Hui, "Multi-objective optimization for hydraulic hybrid vehicle based on adaptive simulated annealing genetic algorithm," *Eng. Appl. Artif. Intell.*, vol. 23, no. 1, pp. 27–33, 2010.
- [11] E. Vinot, V. Reinbold, and R. Trigui, "Global optimized design of an electric variable transmission for HEVs," *IEEE Trans. Veh. Technol.*, vol. 65, no. 8, pp. 6794–6798, Aug. 2016.
- [12] O. Tremblay, L. A. Dessaint, and A. I. Dekkiche, "A generic battery model for the dynamic simulation of hybrid electric vehicles," in *Proc. IEEE Veh. Power Propulsion Conf.*, 2007, vol. 1–2, pp. 284–289.
- [13] H. Sira-Ramirez and R. Silva-Ortigoza, *Control Design Techniques in Power Electronics Devices*. London, U.K.: Springer-Verlag, 2006.
- [14] M. A. Jabbar, A. M. Khambadkone, and Z. Yanfeng, "Space-vector modulation in a two-phase induction motor drive for constant-power operation," *IEEE Trans. Ind. Electron.*, vol. 51, no. 5, pp. 1081–1088, Oct. 2004.
- [15] M. Ehsani, Y. Gao, and A. Emadi, "Electric propulsion systems," in *Modern Electric, Hybrid Electric and Fuel Cell Vehicles: Fundamentals, Theory, and Design*, 2nd ed. New York, NY, USA: Taylor & Francis, 2010.
- [16] P. Vas, *Sensorless Vector and Direct Torque Control*. Oxford, U.K.: Oxford Science, 1998.
- [17] P. Tatjewski, "Supervisory predictive control and online setpoint optimization," *Int. J. Appl. Math. Comput. Sci.*, vol. 20, no. 3, pp. 483–495, 2010.
- [18] M. A. Jirdehi and A. Rezaei, "Parameters estimation of squirrel-cage induction motors using ANN and ANFIS," *Alexandria Eng. J.*, vol. 55, no. 1, pp. 357–368, 2016.
- [19] S. Boyd and L. Vandenberghe, *Convex Optimisation*. Cambridge, U.K.: Cambridge Univ. Press, 2004.
- [20] M. Grant and S. Boyd, *CVX: Matlab Software for Disciplined Convex Programming*, version 2.1, 2014. [Online]. Available: <http://cvxr.com/cvx>
- [21] M. Grant and S. Boyd, "Graph implementations for nonsmooth convex programs," in *Recent Advances in Learning and Control* (Lecture Notes in Control and Information Sciences), V. Blondel, S. Boyd, and H. Kimura, Eds. London, U.K.: Springer-Verlag, 2008, pp. 95–110.
- [22] Y. Li, X. Lu, and N. C. Kar, "Rule-based control strategy with novel parameters optimization using NSGA-II for power-split PHEV operation cost minimization," *IEEE Trans. Veh. Technol.*, vol. 63, no. 7, pp. 3051–3061, Sep. 2014.
- [23] K. Deep, K. P. Singh, M. L. Kansal, and C. Mohan, "A real coded genetic algorithm for solving integer and mixed integer optimization problems," *Appl. Math. Comput.*, vol. 212, no. 2, pp. 505–518, 2009.
- [24] P. Elbert, T. Nüesch, A. Ritter, N. Murgovski, and L. Guzzella, "Engine on/off control for the energy management of a serial hybrid electric bus via convex optimization," *IEEE Trans. Veh. Technol.*, vol. 63, no. 8, pp. 3549–3559, Oct. 2014.
- [25] P. Cominos and N. Munro, "PID controllers: Recent tuning methods and design to specification," *Proc. IEE*, vol. 149, no. 1, pp. 46–53, Jan. 2002.



Arne De Keyser was born in Sint-Niklaas, Belgium, in 1993. He received the M.Sc. degree in electrical and mechanical engineering from Ghent University, Ghent, Belgium, in 2016.

He fulfilled an Internship at the Simulation and Modeling department, ArcelorMittal, Ghent, as a Systems Engineer, in 2015. In August 2016, he joined the Department of Electrical Energy, Metals, Mechanical Constructions and Systems, Ghent University, as a Ph.D. Student of the Special Research Fund (B.O.F.). His research interests mainly concern time-

efficient metamodeling algorithms and robust optimization techniques of complex dynamic systems, focusing on real-time implementation of minimization strategies in hybrid systems containing power electronic elements.

Mr. De Keyser is an affiliate member of Flanders Make, the strategic research centre for the manufacturing industry in Flanders, Belgium.



Matthias Vandeputte was born in Ghent, Belgium, in 1993. He received the M.Sc. degree in electrical and mechanical engineering from Ghent University, Ghent, Belgium, in 2016.

In 2015, he interned at the Simulation and Modeling department, ArcelorMittal, Ghent, as a Systems Engineer. He joined the Department of Electrical Energy, Metals, Mechanical Constructions and Systems, Ghent University as Ph.D. Student of the Special Research Fund (B.O.F.) after graduating, in 2016. His current research interests are semianalytical and numerical methods in electromagnetics, sizing and topology optimization, applied on interacting resonant structures.

Mr. Vandeputte is an affiliate member of Flanders Make, the strategic research centre for the manufacturing industry in Flanders, Belgium.



Guillaume Crevecoeur was born in Ghent, Belgium, in 1981. He received the M.Sc. degree in physical engineering and the Ph.D. degree in applied sciences from the Ghent University, Ghent, Belgium, in 2004 and 2009, respectively.

In 2004, he joined as a Doctoral Researcher the Department of Electrical Energy, Metals, Mechanical Constructions and Systems of the Faculty of Engineering and Architecture, Ghent University. Since 2009, he has been a Postdoctoral Researcher for the Fund of Scientific Research-Flanders (FWO) at

Ghent University. In the winter of 2011, he was a visiting researcher at the Technical University Ilmenau and the Physikalische Technische Bundesanstalt, Berlin, Germany. In October 2014, he was appointed Associate Professor in the research field modeling, optimization and control of electrical energy applications.

Dr. Crevecoeur is a member of Flanders Make, the strategic research centre for the manufacturing industry. His main research interests are multidomain modeling, inverse problems, data analytics, numerical optimization, co-design, uncertainty quantification, numerical and experimental mechatronics.